ELSEVIER

Earth and Planetary Science Letters 159 (1998) 99–115

EPSL

Detection of mantle plumes in the lower mantle by diffraction tomography: Hawaii

Ying Ji, Henri-Claude Nataf *

CNRS URA 1316, Départment Terre–Atmosphère–Océan, Ecole Normale Supérieure, 24, rue Lhomond, 75231 Paris Cedex 05, France

Received 14 April 1997; accepted 24 March 1998

Abstract

A new method is proposed to detect mantle plumes in the lower mantle. The method is akin to diffraction tomography, and relies on the scattering of long-period seismic body waves by nearly vertical heterogeneities. The theory is described in a companion paper [Ying Ji, H.-C. Nataf, Earth Planet. Sci. Lett., this issue]. Here we apply this method to an actual set of long-period digital seismograms recorded on the world-wide network of seismic stations between 1980 and 1994. We select seismograms that 'illuminate' the lower mantle in a $20^o \times 20^o$ region around Hawaii. We construct an image of 'plume-like' heterogeneities, using a cell size of $1^o \times 1^o$, by a LSQR inversion of the scattered waves. This image shows a strong slow anomaly about 200 km northwest of Hawaii. Although the image is somewhat noisy, resolution tests indicate that this feature is fairly robust. The amplitude of the anomaly is between 30 and 60 times larger than what we predict from a simple thermal plume model, built with a 600 K maximum temperature excess, and a gaussian horizontal cross-section with an $1/e$ diameter of 250 km. It is the first time that such a method is applied to the mantle. While we think that the existence of this anomaly is real, we do not know how to explain such a large amplitude. If real, this observation has a number of important geodynamical consequences. It indicates that a mantle plume is indeed responsible for the Hawaii hotspot, as speculated by Morgan [W.J. Morgan, Nature 230 (1971) 42–43]. The plume is nearly vertical. It originates from the D″ region, at the base of the lower mantle. The amplitude of the anomaly suggests that partial melt or/and a chemical anomaly must be present. The plume source is to the northwest of its surface expression, as predicted by some models of plume advection in the 'mantle wind'.

Keywords: diffraction; tomography; mantle plumes; Hawaii; hot spots

1. Introduction

In 1963, Tuzo Wilson [1] proposed that the linear chain of volcanoes northwest of Hawaii was the track left by a 'hot spot' fixed beneath the moving lithosphere, the hot spot being now responsible for the volcanic activity on Hawaii. Jason Morgan [2] speculated that the fixed hotspot source was a thermal plume rising through the mantle, from some unstable boundary layer, possibly at the base of the mantle. Since then, many more hotspots have been 'identified' (see [3] for a review). The mantle plume hypothesis is now widely accepted, despite the lack of firm evidence for an actual plume beneath any hotspot.

The pioneer work of Iyer et al. [4] showed evidence for slow material below the Yellowstone hotspot down to 250 km. Recently, spectacular images of

* Corresponding author.
E-mail: henri-claude.nataf@obs.ujf-grenoble.fr

0012-821X/98/$19.00
PII S0012-821X(98)00060-0

plume-like columns in the upper mantle have been obtained, using travel-time tomography, beneath the French Massif Central [5], the Parana Basin [6], and Iceland [7]. The evidence for a deeper signature is more elusive. A detailed study of travel-time anomalies led Nataf and VanDecar [8] to the conclusion that a plume was present 700 km beneath the Bowie hotspot. An early account of a large anomaly at the core–mantle boundary (CMB) beneath Hawaii from the analysis of P-wave slowness at the LASA seismic array [9] was soon dismissed [10].

There is no doubt that constraints on the deep structure of hotspots would be of great help to know their origin, and to understand the dynamics of the mantle. In this study, we apply a new tomographic method, which relies on the scattering of long-period body waves by nearly vertical narrow structures in the mantle. This theory, together with forward modelling on a plume-like structure, is developed in Ji and Nataf [11], a companion paper hereafter referred to as paper I.

This article is organized as follows: Section 2 presents the data and data selection procedure; Section 3 gives the maps of the heterogeneities beneath Hawaii; in Section 4 we perform several tests to assess the reliability of these maps, and the potential of our theory; Section 5 discusses the results; Section 6 speculates on possible geodynamical implications.

2. Data

In this study, we apply the theory developed in paper I to long-period seismic records that contain potential informations on plume-like scatterers beneath the Hawaiian region. We use the large data set of digital records for the years 1980–1994. For the years 1980–1987, records are from the Global Digital Seismograph Network (GDSN), available on CD-ROMs. For the years 1988–1994, we retrieve the seismograms from the Data Management Center of the Incorporated Research Institutions for Seismology (IRIS).

We selected the long-period channels of stations that record the three components of ground motion, sampled at 1 Hz. We used seismograms from 39 different stations here. Only the vertical component is analyzed.

We only consider earthquakes shallower than 50 km, in order to avoid the contamination of the P-coda by surface reflections. We have a total of 1927 events, but only a fraction will contribute to our region of interest.

Records are then selected according to epicentral distance, which must be larger than about 45°, so that P and PP are separated by more than 110 s, and smaller than 100°. In this distance range, classical ray theory can be used to compute synthetic seismograms. We keep earthquake-station pairs for which the records carry information on the region of interest (here around Hawaii), within the theory developed in paper I.

The data treatment and selection proceed with the following steps. (1) The seismograms are all transferred to a common instrument response (ANMO LP), and band-pass filtered around 20 s. (2) The amplitude of the direct P-wave is estimated by measuring the maximum amplitude in a time window starting 40 s before the theoretical arrival time, and ending 60 s after. The noise level is determined from the amplitude recorded in the 40-s window preceding the observed P-wave arrival time. We reject the records for which the signal-to-noise ratio is less than 10. (3) We construct a synthetic waveform of the direct P-wave by adding the contributions of the P, pP, and sP waves. This is done using ray theory, and the source parameters given by the centroid moment tensor (CMT) from Harvard. Seismograms for rays close to a node are discarded. (4) The synthetic waveform is cross-correlated with the data. The time of the maximum correlation gives the time correction to be applied to the record. Records with a maximum correlation smaller than 0.75 are discarded. (5) In order to avoid contamination of the images by outliers (when a record contains a strong arrival after the direct P-wave), we remove records for which the amplitude in the time window (0, 60 s) is less than twice that in the (60 s, 100 s) window, where the time reference is the P arrival time.

A word is needed concerning the treatment of waves diffracted at the core–mantle boundary. This is never the case for the direct P-wave in the distance range we consider. The scattered wave can travel as a diffracted wave on part of its path. However, we exclude from the inversion cases for which the fastest ray of paper I is a diffracted wave. When we

compute the synthetic scattered wave, we only count the contributions of the plume from non-diffracted waves, as we expect these to contribute little to the total scattered wave.

We applied this data selection scheme to image the mantle around Hawaii. In the following, we build images for $10^o \times 10^o$ and $20^o \times 20^o$ squares around Hawaii. In both cases, the unit cell is $1^o \times 1^o$. The total number of selected seismograms is 261 for the former, and 670 for the latter. Fig. 1 shows the hit-count map of the $1^o \times 1^o$ cells for these two cases. We see that the coverage is rather homogeneous, with a hit count everywhere larger than 50.

Fig. 2a gives the distribution of the data as a function of epicentral distance for the $10^o \times 10^o$ case. Most data are in the range 75^o to 95^o. As shown in paper I, the intersection depth of the scattered wave with a vertical scatterer is mostly a function of the epicentral distance. Fig. 2b shows the expected depth sensitivity of the waves we analyze to plume-like features in the mantle. We see that most data sample the lowermost part of the lower mantle.

Fig. 3 shows the ray paths of scattered waves that sample the anomaly we get near Hawaii. We use an azimuthal projection centred on (-157^o, 22^o). In this projection, the great circle paths from source to plume and from plume to station are straight lines. Also drawn are small circles at distances of 25^o, 50^o, 75^o, and 120^o (outer rim). Note that the rays illuminate three quadrants.

Fig. 4 shows a selection of the actual seismograms used in the inversion. The records are aligned on the observed P arrival. Also indicated is the theoretical arrival time (with respect to P) of the PP wave.

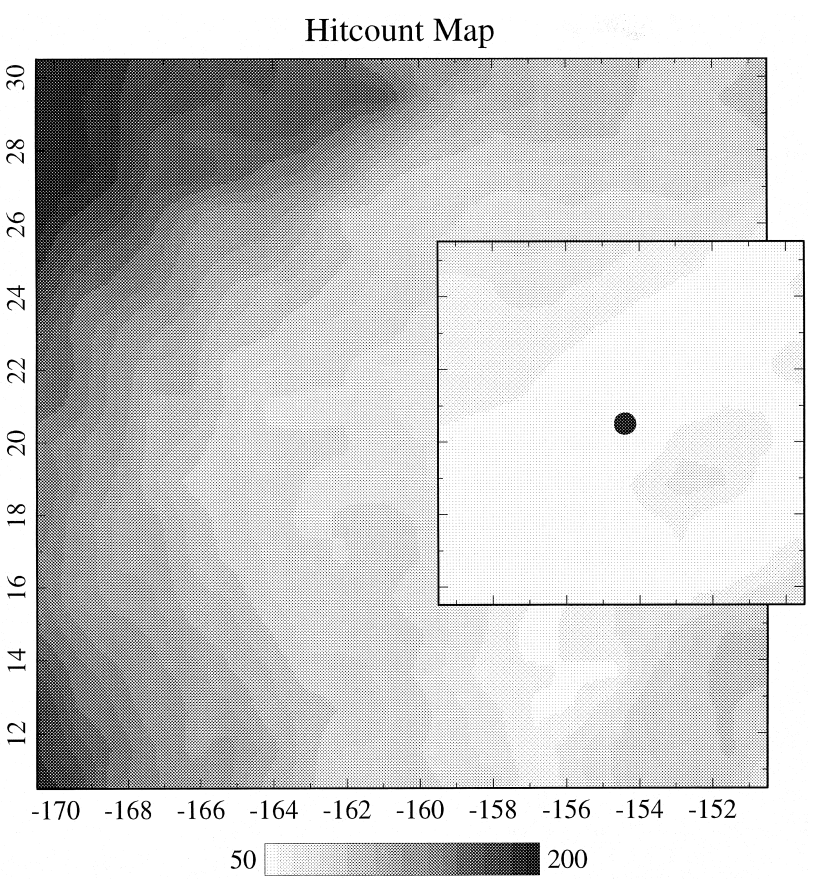

Fig. 1. Hit-count map around Hawaii. The map displays the number of rays that 'hit' a $1^o \times 1^o$ cell. The large map is our $20^o \times 20^o$ grid. It is overlapped by the hit-count map for our $10^o \times 10^o$ grid. The position of the Hawaii hotspot (taken at -154.4^o, 20.5^o) is indicated by the black dot. The hit-count is everywhere larger than 50. These two grids are used throughout this paper.

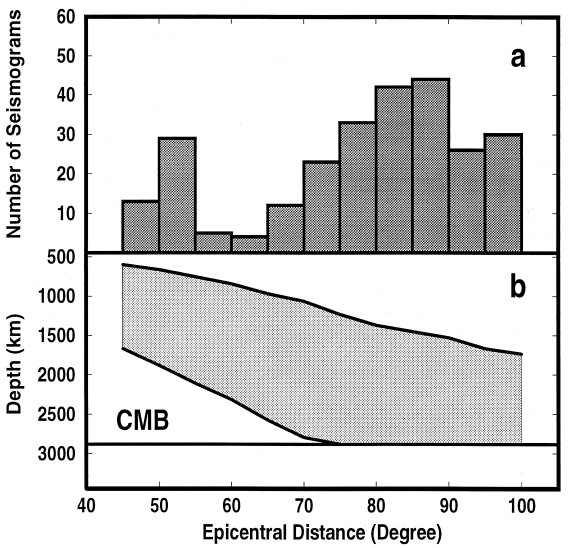

Fig. 2. (a) Histogram of the number of seismograms as a function of epicentral distance, for the actual $10^o \times 10^o$ inversion around Hawaii. (b) Sampling depth ($T/6$ Fresnel zone) of vertical heterogeneities as a function of epicentral distance, in the framework of the theory developed in paper I. Note that the majority of the seismograms sample the lowermost lower mantle.

We observe scattered energy, with amplitudes up to 50% of the direct P wave, arriving between P and PP. We note that in all cases, this energy is much larger than the noise deduced from the amplitude of the seismogram before the P arrival. It is also much larger than the few percents predicted for scattering by the reference plume of paper I. The stack of 44 records at the bottom indicates that there is no coherent energy linked with the arrival of the direct P-wave in the time-window used in the inversion.

3. Images of the Hawaiian plume

We apply the diffraction tomography method described in paper I to the selected data set. We take the time window (55 s, 90 s) after the observed direct P-wave arrival, and apply a 5 s cosine taper to both ends. The choice of this time window results from a compromise: it should be as close as possible to the direct P, so that the amplitude of the scattered wave is large, but it should not be contaminated by the direct P itself. We minimize the misfit between one frequency component of the data in this window, both phase and amplitude, and the corresponding component for the synthetics. The chosen frequency component corresponds to a period of 20 s. The synthetics are computed according to the method described in paper I, and are submitted to the same processing as the data (filtering, tapering, etc.). The radial earth model is iasp91 [12]. The damping constant Λ of paper I is 5. Tests reveal that the choice of this parameter is not crucial.

We now present the maps of heterogeneities inverted from the data for the Hawaiian region. It is important to recall the main assumptions made. (1) The scatterers are predominantly vertical, and therefore the tomographic problem reduces to a 2D problem. (2) The contributions to scattering of ρ, α, and β are all lumped into a heterogeneity of temperature, with the relations given in paper I. (3) The data are cross-correlated with synthetics computed under the hypotheses of Born and Rayleigh scattering by a line. (4) The amplitude variation of the scattered wave is a function of the time separation between the direct P wave and the scattered wave, as determined in paper I.

Under these assumptions, we construct a 2D image of scattering thermal heterogeneities around Hawaii, expressed in 'plume units'. In these units, our reference thermal plume, with $\Delta T = 600$ K and $1/e$ radius 125 km, and the temperature derivatives of paper I should be 1.

If real, these results could deeply renew our views on mantle plumes, and modify the methods used in tomography. Before discussing such implications, and addressing the problem of the very large amplitudes we obtain, we need to check the reliability of these images.

4. Tests and resolution

In this section, we perform several tests in order to check that the images we produce are indeed constrained by the data, and are not an artefact of the imaging technique. In all the synthetic tests to follow, we keep the same earthquake-to-station pairs as in the real case. The inversion procedure and parameters are also identical. When synthetics are computed, we use the method described in paper I, with a plume extending from the surface to the core mantle boundary.

Fig. 3. Ray paths of the scattered waves that sample the anomaly we get near Hawaii. There are 261 rays, corresponding to the $10^o \times 10^o$ map. The azimuthal projection is centred on the anomaly at (-157^o, 22^o). The great circle paths between source (crosses) and plume, and between plume and station (triangles) are straight lines. Small circles centred on the 'plume' drawn at 25^o, 50^o, 75^o, and 120^o. Note that the anomaly is illuminated from many sides.

4.1. Sensitivity to noise

In the first test, we introduce a unit vertical plume at the two locations (-157^o, 22^o) and (-158^o, 23^o) where we found a large slow anomaly in the real image. The rest of the $10^o \times 10^o$ grid is devoid of scatterers. We then construct synthetics with the theory of paper I for all seismograms, and perform the inversion. Fig. 7a shows that the two plumes are very well recovered in the absence of noise. The number of retained seismograms is 261 in this case, as for the real data. Fig. 7b and c show the deterioration of the image as noise is added to the data. When the noise level reaches 80% of the scattered wave, the image is severely distorted, but the two 'plumes' are still visible. We conclude that the effect of unmodelled waves, such as near station scattering, PcP waves, or body-wave to surface-wave conversion, should not deteriorate our 2D image of plume-like scatterers, as well as the scattered waves by the anomalies outside the region we inverted, as long as their amplitude is no more than about 50% of the scattered wave itself. In other words, if the amplitude of the unmodelled waves is larger than 50% of the waves scattered by

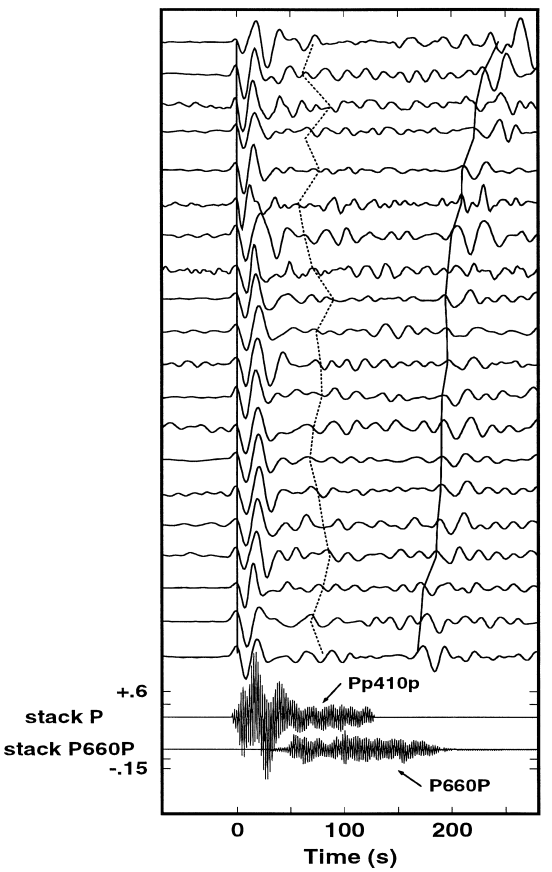

Fig. 4. Examples of the actual seismograms used in the inversion of scattered waves sampling the anomalous region beneath Hawaii. All records are aligned on the direct P wave (marked with the straight line), and normalized to the observed amplitude. The epicentral distance increases from about 75° at the bottom to 100° at the top. The PP wave theoretical arrival is indicated by a solid line. Note the energy between these two waves. We apply diffraction tomography to the time window (55s, 90s) after the P wave (dashed lines). The dotted line is the reference time used in Fig. 11 (see text). At the bottom are drawn the stacks of all 44 seismograms which sample that point, aligned on the arrival time of the observed P wave (P-stack), and on the expected arrival time of the P660P wave (P660P-stack). The thickness of the line is 2σ.

the vertical anomalies, we cannot obtain a robust image.

4.2. Spatial resolution

The previous test showed that the spatial location of the plume is well recovered, even when noise is added. Of course, resolution depends upon position. We perform a second synthetic test, in which a unit plume is positioned every odd degree in latitude, and every even degree in longitude. This test is often called the spike sensitivity test [15]. Fig. 8 gives the image retrieved for this array of plumes (noise-free synthetics). All plumes are well recovered, with their correct amplitude. This shows that the back projection is efficient, and the data coverage sufficient for a good recovery over the full $10^o \times 10^o$ grid.

4.3. Split data set

Fig. 6 shows the $20^o \times 20^o$ map. It is again dominated by a slow anomaly in the same position as in Fig. 5a, but with a smaller amplitude of 35 plume units. A strong anomaly is also visible at the northern rim of the map. The western rim displays what looks like numerical instabilities.

The diagnostic value of the tests performed with synthetics is limited by several problems [15,16]. First, the scattered ray geometry adopted in the inversion is the same as the one with which the synthetics are computed. In the actual Earth, long-wavelength heterogeneities can displace the Fermat rays by several hundred kilometres. This, in turn, can affect the image reconstruction. Secondly, the addition of normally distributed noise to the synthetics does not necessarily mimic well the statistical properties of real data errors, because many sources of systematic errors exist.

It is therefore useful to complement these tests with exercises performed with the actual data. In that case, of course, the real model is not known, but the internal consistency of the inversion can be addressed. One such simple exercise consists in splitting at random the original data set in two half-size sets, and comparing the results of the two separate inversions (e.g. [17]). Fig. 9 shows the two images thus constructed with two data sets of 180 records. We could not take completely independent data sets because the total number of records is only 261, and it was not possible to construct an image with only 130 records. However, only 50 records are common to the two sets. The main features of the original image are recovered, and in particular the slow anomaly northwest of Hawaii (with a slightly weaker amplitude). The background level is

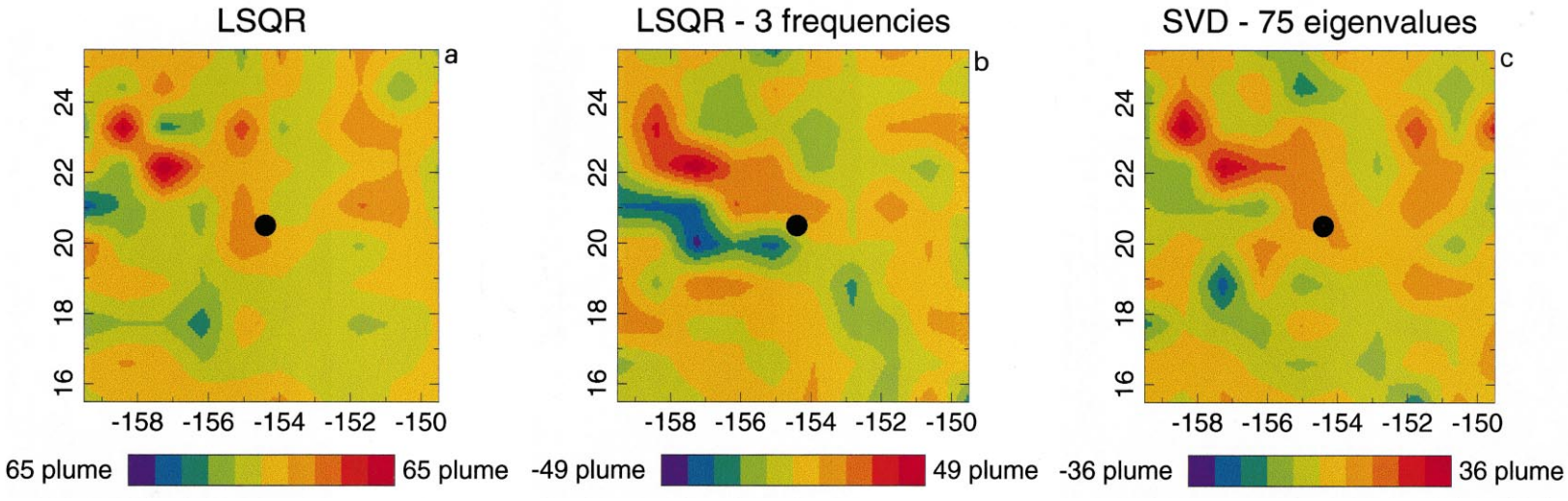

Fig. 5. Images of scattering heterogeneities in the lower mantle in the region beneath Hawaii (marked by a black dot). The intensity of the scatterers is given in 'plume unit' (see text). (a) $10^{o} \times 10^{o}$ image from LSQR inversion of a single frequency. (b) Image from LSQR inversion of three frequencies (periods of 25.6 s, 17.1 s and 12.2 s). (c) Image from SVD inversion with the 75 largest eigenvalues kept. In all maps, the grid element is $1^{o} \times 1^{o}$. The apparent interpolation is only for graphical representation. A double slow anomaly is clearly visible in all maps northwest of Hawaii.

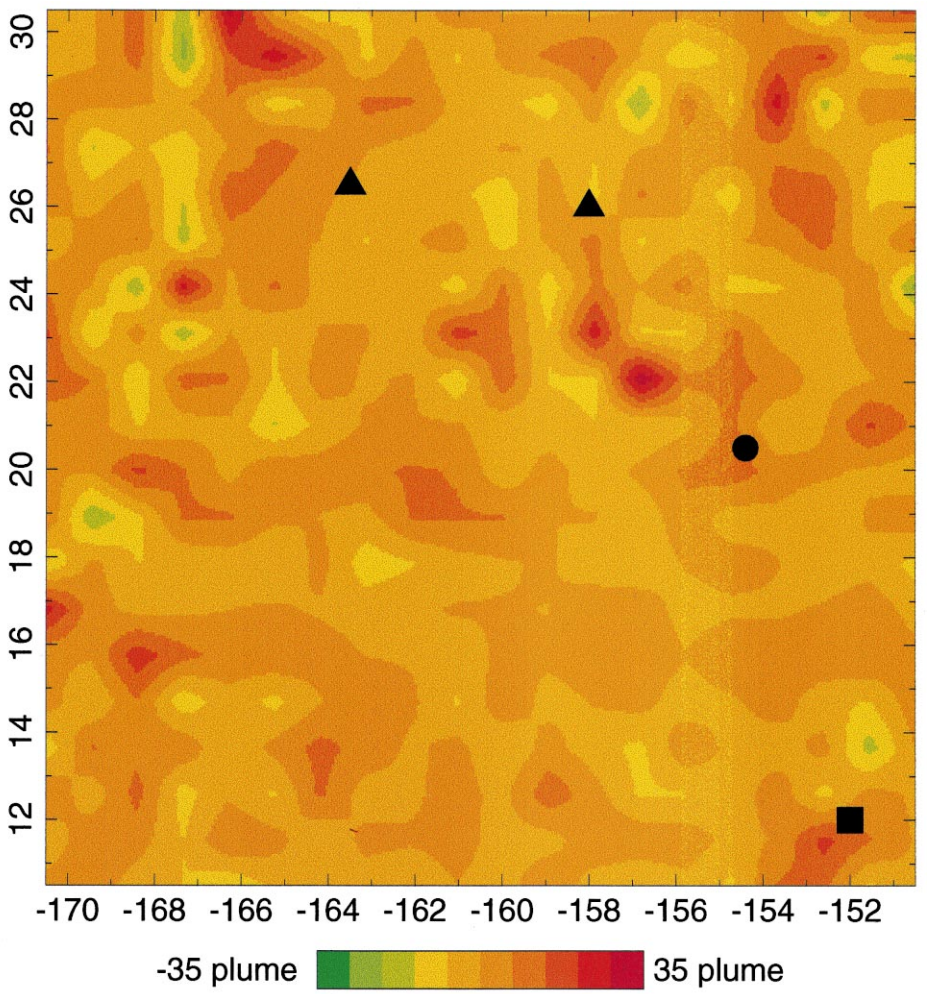

Fig. 6. Same as Fig. 5a but for our 20° × 20° region around Hawaii. Also drawn are the predictions of the position of the Hawaiian plume source at the CMB, according to Corrieu-Sipahimalani [13] (black triangles), and to Steinberger and O'Connell [14] (black square).

larger than in Fig. 5a. We conclude that the slow anomaly detected northwest of Hawaii is a robust feature.

4.4. Permuted data

Another popular test can be applied to real data. The game is to destroy the correspondence between the paths and the data by a random permutation of the seismograms (e.g., [15]). The falsified data are then inverted to form an image. Ideally, one expects a very noisy image, with rather small amplitudes. In practice, the interpretation of this test is not obvious [18]. Fig. 10a shows the image we obtain for one particular realization of the random permutation. It is rather noisy, as expected, but the amplitudes are only slightly lower than for the real case (see Fig. 5a). This could mean that we are making images out of 'random' noise in the seismograms. However, if we compute synthetics using the actual inverted model of Fig. 5a, and permute the seismograms according to the same realization as previously, we obtain the image shown in Fig. 10b. This image is very similar to the previous one, which indicates that the inversion is giving an image that adequately transfers the information available in the data.

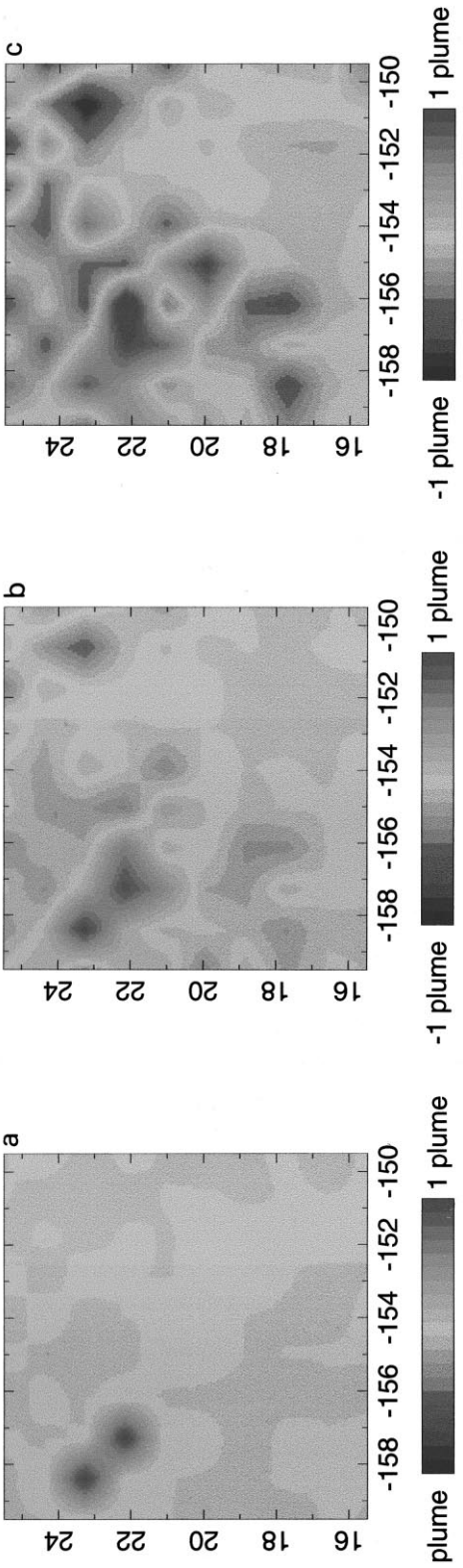

Fig. 7. Images constructed from synthetic data. The earthquake to station pairs are the same as for the real data. The input model consists in unit plumes placed at (−157°, 22°) and (−158°, 23°). (a) No noise added. (b) 30% noise. (c) 80% noise. In all cases, the plumes are recovered, but artefacts become strong for the high noise level.

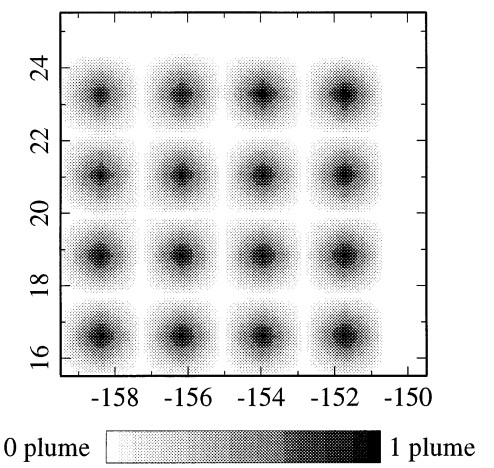

Fig. 8. Spike sensitivity test. The input model consists of an array of plumes, spaced by 2°. The image constructed from the noise-free synthetics shows that all plumes are very well recovered.

4.5. Multiple frequencies

All the results above were obtained using only one frequency component. We now look at the effect of introducing additional frequencies. Since the band of the instrument response plus filter is quite narrow, we only choose three frequency components, at 25.6 s, 17.1 s and 12.2 s, respectively, to be included in the inversion. Fig. 5b shows the result. The main features are very similar to those of Fig. 5a, but with smaller amplitude and a stronger background noise level. This test indicates that adding more frequencies does not bring new information. On the other hand, it demonstrates that the image is robust since it is not affected by the inclusion of different frequency components, which are clearly separated in phase.

4.6. Fit to the data

The test with synthetic permuted data presented above demonstrates that the inverted model provides a good fit to the data. One can get a feeling of this fit by looking at the actual seismograms. In Fig. 11, we present the same seismograms as in Fig. 4, except that they are now aligned on the predicted arrival time of a P wave that would be scattered by a vertical heterogeneity at (−157°, 22°),

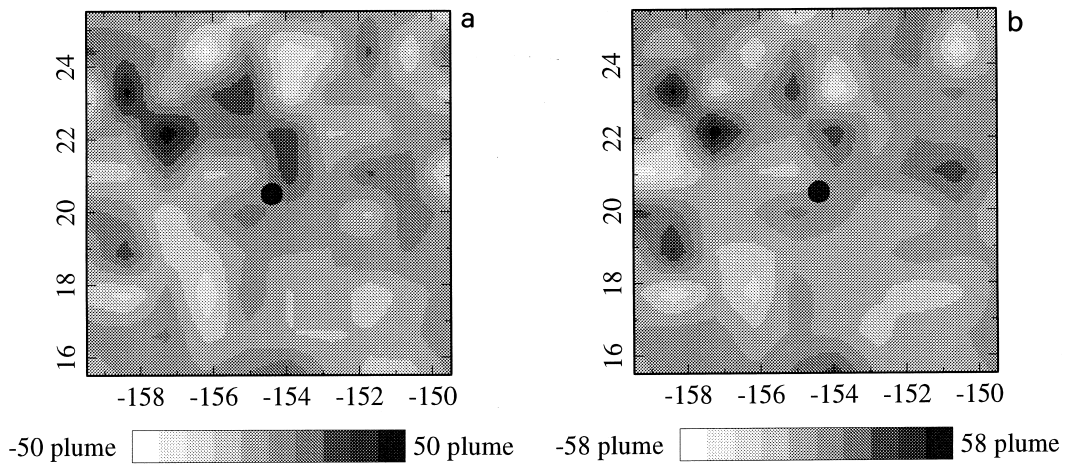

Fig. 9. Split data sets: (a) and (b) are two images constructed from two partial data sets of 180 records only. 50 records are common to the two data sets. The distribution in the two sets is random. Note that the slow anomaly northwest of Hawaii is present in both maps.

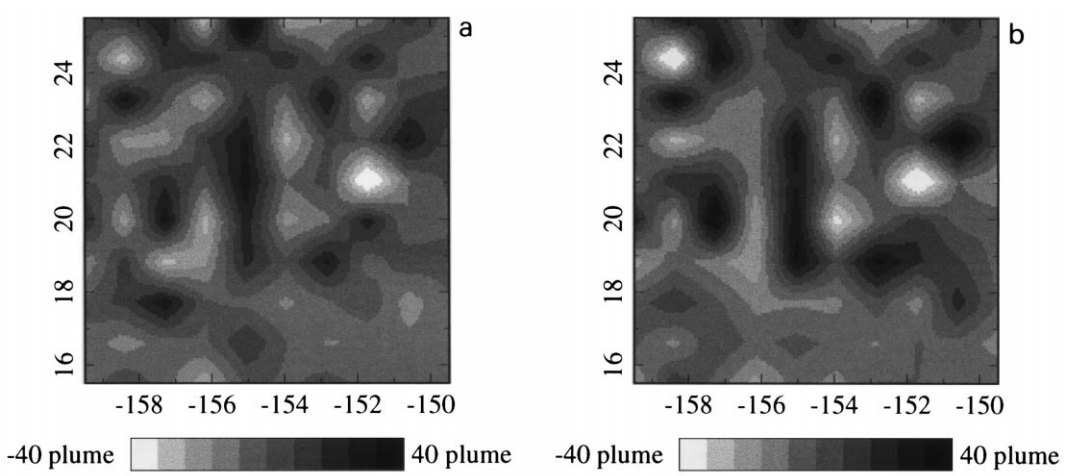

Fig. 10. Permuted data set. (a) Image constructed from randomly permuted data. (b) For the same realization of the permutation, the data are replaced by synthetics computed using the model of Fig. 5a as the input model. Note that the 'actual' and synthetic images are very similar.

where we find the largest slow anomaly. The sign and amplitude are scaled to the predicted ones. We observe that most seismograms are in phase around the predicted arrival time of the scattered wave, with a large negative swing just behind. This is clear when we consider the stack of all 44 seismograms which sample that point. It is drawn at the bottom of Fig. 11, with its 2σ thickness. To be compared, we plot the stack of the same 44 seismograms, but aligned on the observed P wave arrival time at the bottom of Fig. 4. It is rather clear that there exist some coherent signals in the stack aligned on the predicted arrival time of the wave scattered by the vertical plume we found.

4.7. Stack

The same stacking method can be used to compute all points of our $20^{o} \times 20^{o}$ map, as shown in Fig. 12. Again, we find some strong signals around $(-157^{o}, 22^{o})$. The maximum amplitude of the stack is about 15% of the direct P wave. The rms analysis

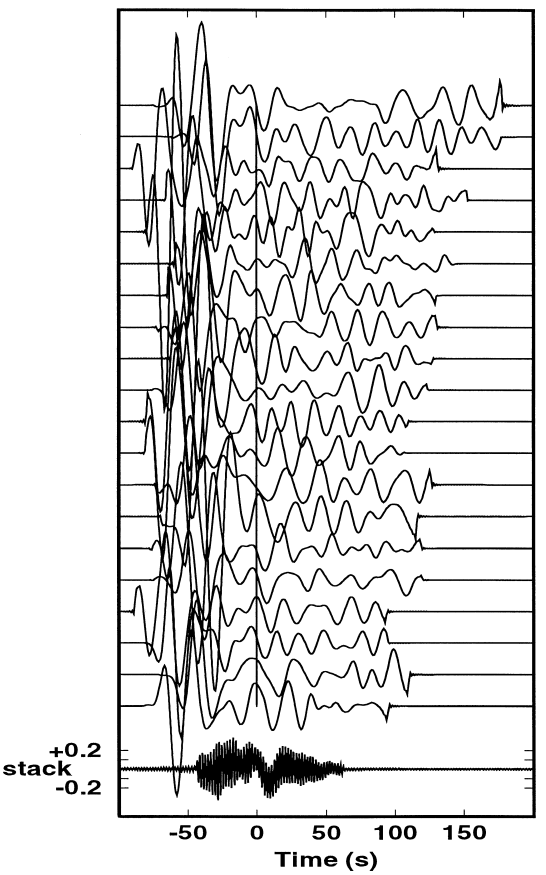

Fig. 11. Same seismograms as in Fig. 4, aligned on the predicted arrival time (vertical line) of a P wave scattered by the main slow anomaly found northwest of Hawaii at (−157°, 22°). The amplitudes and sign are also scaled to the predicted ones. The records have been transferred to a unique instrument response, and filtered around 20 s. Note that most seismograms tend to be in phase around the predicted arrival time. At the bottom is drawn the stack of all 44 seismograms which sample that point, aligned in the same way. The thickness of the line is 2σ. The large negative swing is very clear. It is responsible for the slow anomaly detected northwest of Hawaii.

reveals that only the slow spot northwest of Hawaii is above the noise level.

4.8. Singular value decomposition

Since the stacks and the maps we produce are rather noisy, one may wonder whether they are really resolved. For our $10^o \times 10^o$ inversion, the number of unknowns is 100, while the number of data is 261. While the tests with synthetics indicate that this is quite enough to produce a good image when the noise level is low (see Fig. 7) this might not be the case for the actual data. The Singular Value Decomposition (SVD) method enables to address this problem. As mentioned in paper I, LSQR is better suited for the large and sparse systems that appear in large-scale tomographic imaging, but we can perform SVD for our small $10^o \times 10^o$ inversion. The idea is to find the actual number of unknowns that can be resolved from the available data, and to build a model using only these resolved unknowns (which are linear combinations of the grid elements).

We have applied the SVD scheme to both data and synthetics. The data have been treated following two different philosophies. In the first one (1), we keep the amplitude of the original seismograms and simply correct for instrument response, focal mechanism, geometric spreading, and scattering as previously, so that larger signals are given more weight. In the second one (2), we scale the direct P of all seismograms to 1, thereby assuming that all 'noise' perturbing the scattered wave is proportional to the direct P. The noise-free synthetics are computed for the model obtained from the inversion of the data treated according to the first method, and displayed in Fig. 5c.

Fig. 13a gives the data misfit (root mean square over initial root mean square) and Fig. 13b the model norm (square root of the sum of the model elements squared), as a function of the number of retained eigenvalues, for all three cases. As expected, the misfit decreases and the model norm increases as the number of retained eigenvalues increases. Synthetics and data show rather similar trends. The final misfit is much larger for the data treated following the second approach. As often in tomographic problems, the results for the noise-free synthetics show that one needs to keep almost all eigenvalues in order to recover fully the original amplitude (100 in these units).

Ideally, we would like to stop the SVD inversion at a rank beyond which the misfit falls below the noise level. In practice, however, we do not know where the noise level sits. If we rely on our predicted amplitudes for a thermal plume, then most of our 'signal' is noise and we should stop the inversion very soon, thereby obtaining a very low amplitude unresolved model. However, if the signal is as large as we find in the inverted models, then

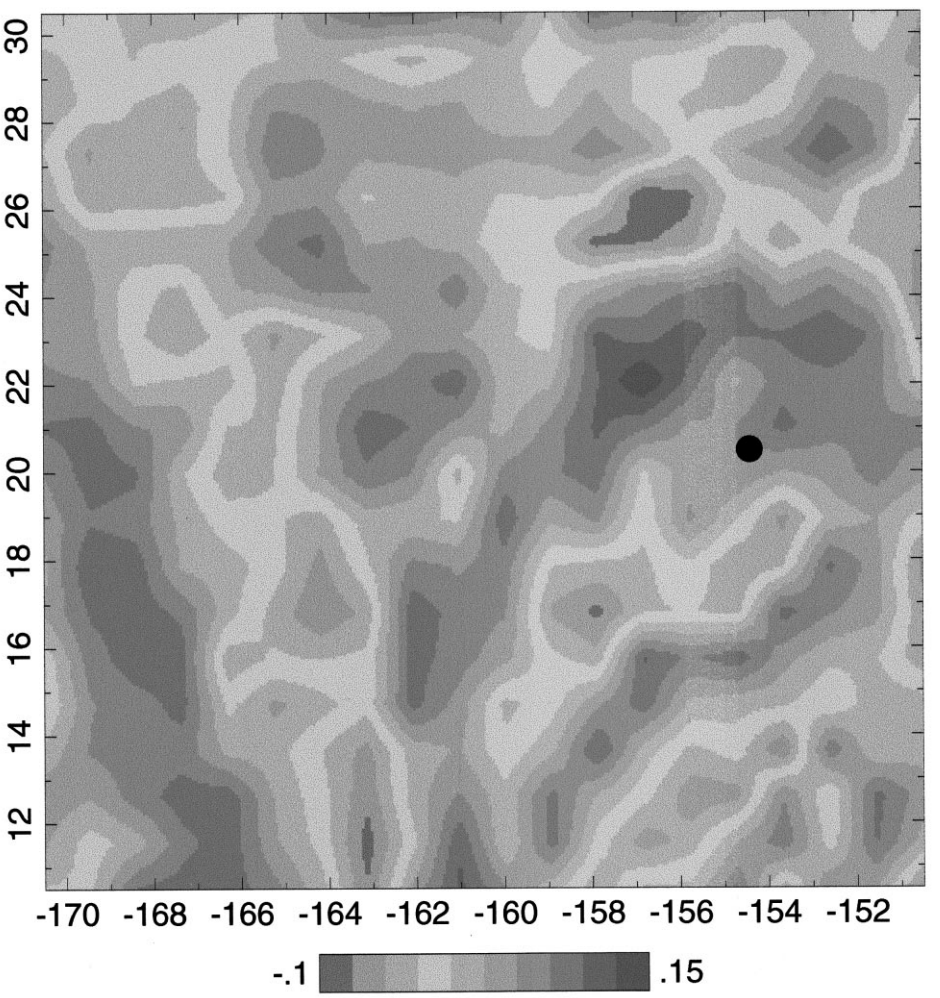

Fig. 12. 20º × 20º map of heterogeneities in the lower mantle beneath Hawaii by using the same stacking method used to compute the stack at the bottom of Fig. 11.

the noise could be quite low, and we should keep most eigenvalues. In Fig. 5c, we show the model obtained from the SVD inversion of the data treated according to our first philosophy if we retain only the 75 largest eigenvalues. The model is similar to our LSQR result, with a lower amplitude. The double slow anomaly northwest of Hawaii is still the dominant feature.

5. Discussion

The synthetic tests we have presented demonstrate that the method developed in paper I provides an excellent resolution of plume-like features, given the actual distribution of available digital long-period seismograms. We have constructed the first 2D image of vertical heterogeneities in the lower mantle beneath Hawaii. This image is dominated by a double slow anomaly a few degrees northwest of Hawaii. Before dwelling into the possible geodynamical implications of this finding, we need to discuss several issues it rises.

5.1. Is the anomaly real?

The key question is: are we sure that the image we build has something to do with the actual

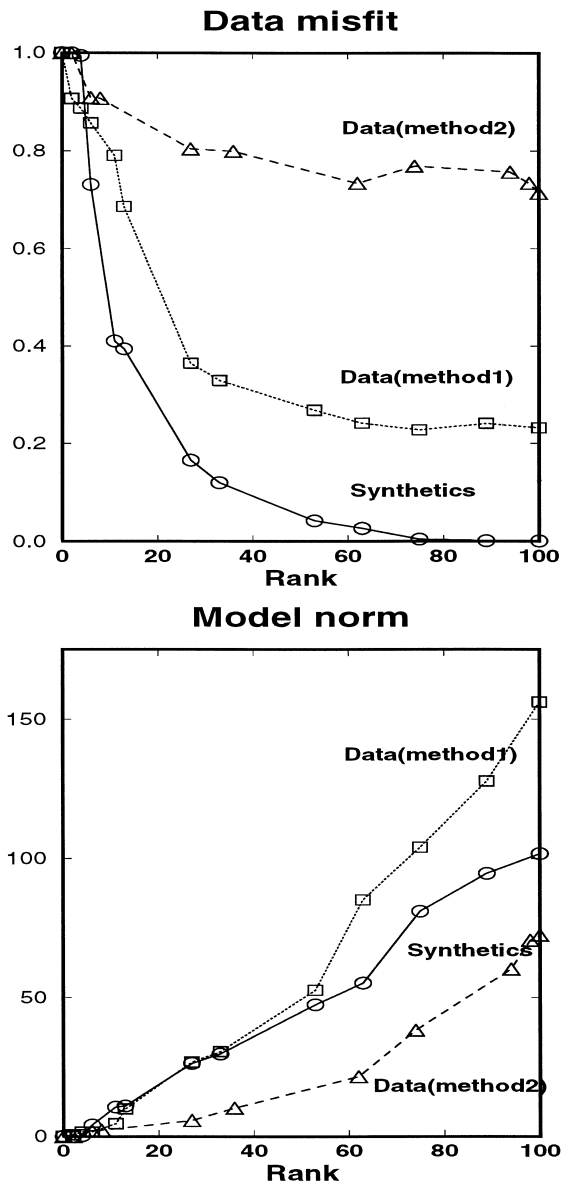

Fig. 13. Singular value decomposition results for our $10^o \times 10^o$ case ((1) and (2): see text), and for the corresponding noise-free synthetics. (a) Normalized misfit as a function of the number of singular values kept. (b) Inversion model norm as a function of the number of singular values kept.

heterogeneities in that region? The possibility exists that we are back projecting on our image 'noise' of a completely different origin. Other arrivals are indeed expected and observed in the P-coda, in particular P-waves that interact with the upper mantle discontinuities, such as P660P or Pp660p (e.g., [19]). In our distance range, the expected amplitude of these waves is only about 5% of the direct wave. The stacks at the bottom of Fig. 4 show that, in our data set, both families (Ppdp with almost no move-out with respect to P, and PdP such as P660P) stack less coherently than when we align seismograms on the expected times for scattering by the 'plume' anomaly (Fig. 11). Near-source and near-station P-wave scattering by volume heterogeneities are found to be too small [20]. One can also think of P-to-Rayleigh conversions at the surface or at the Moho near the stations. This mechanism is responsible of much of the PP-coda in some cases [20]. However, it is much less efficient for the steep incidence P-waves we are considering [20]. Furthermore, by back projecting the data into our 2D map, we tend to cancel out these contributions, just as they are assumed to cancel out in the conventional stacks for horizontal reflectors. It seems clear that the slow anomaly we find northwest of Hawaii is a robust feature. We find it in the $10^o \times 10^o$ and $20^o \times 20^o$ LSQR inversions, in the SVD inversion with 75 eigenvalues, in the split data set test, in the multiple frequency inversion, and in the stack map (Figs. 5, 6, 9 and 12). Note that by the same token, all other anomalies are not robust. Nevertheless, there are at least three reasons that should keep us sceptical. (1) The stack of Fig. 11 is noisy (although not much more than conventional stacks for horizontal reflectors, e.g. [21]). (2) The amplitude in the coda is not rapidly decreasing with time as predicted for scattering by a vertical line. Of course, this could just mean that other phenomena are taking over progressively (reflections and conversions from horizontal discontinuities, multiple scattering, etc.). (3) The test with permuted data shows that large scatterer amplitudes can be obtained from randomly shuffled data (Fig. 10a). At this stage, it is not possible to be sure that the anomaly we find northwest of Hawaii is real.

5.2. Why is the anomaly so large?

Another key question concerns the amplitude of the anomaly we detect. In paper I, we predict that the amplitude of the waves scattered by a thermal

plume only reaches a few percents of the amplitude of the direct P-wave. As shown in Fig. 4, the typical amplitudes between P and PP are more like 20 to 30%. Our synthetic tests with noise added, as well as the SVD inversion, show that it would not be possible to extract a plume-related signal of only a few percents out of this large amplitude coda. As a consequence, this large amplitude signal translates into a slow anomaly of 30 to 60 'plume-units'. This is at odds with the predictions of paper I.

There are three possible solutions to this paradox: (1) the signal we are back projecting has nothing to do with P-waves scattered by vertical heterogeneities; (2) the heterogeneity due to a plume is much larger than what we estimated; (3) the theory grossly underestimates the amplitude of the scattered wave.

Concerning the first possibility, it is interesting to note that this argument has been used to exclude body-wave scattering as the source of the P-coda: it would require too strong or too large scatterers [20]. This is not so true in the case we consider, because the assumed large vertical extent of the plume boosts the signal, as shown in paper I. Ironically, it is often admitted among delay-time tomographers that the simplicity of long-period seismograms supports the view of a mantle dominated by long-wavelength features. The truth is that, if there are strong localized velocity anomalies of the kind we map, they would not be seen in classical tomography, because of wavefront healing [8,22], and they would not scatter short-period waves efficiently. These remarks cannot dispense us from examining if the large amplitudes we find are geophysically realistic.

It is clear that the plume model we built in paper I is a minimal model. The predicted maximum P-wave velocity anomaly is only 1.8%. It is conceivable that the radius, the temperature anomaly, and the coefficients that relate it to the elastic coefficients, are all somewhat larger than what we chose. It is likely that the temperature derivatives proposed by Stacey are under-estimated by a factor of two [23]. Alternatively, there could be other sources (chemical for example) of heterogeneity. After all, lateral heterogeneities up to 10% are reported [24] in the D″ layer, where plumes might be coming from. Nevertheless, it seems difficult to account for more than a factor of 10 even if all parameters were underestimated in paper I.

The third possibility cannot be ruled out completely. As far as we know, our own predictions of paper I are the only ones we can relate to. It is important to note that in the realistic geometries we investigated, the scattered rays depart from a region of low amplitude of the scattering radiation pattern (see fig. 2 of paper I), a fact that is ignored in all isotropic scattering theories. Had we assumed isotropy, the predicted amplitudes would have been increased by a factor of about four. Also note that we have used the Born approximation in the forward modelling. It is not sure that this is a good approximation for our problem (see Gritto [25]). While it probably yields the correct kinematic behaviour, the amplitude evaluation is more delicate (see [26,27]).

Again, it is not possible to exclude the possibility that the large-amplitude anomaly we detect northwest of Hawaii is an artefact. On the other hand, there is such a long tradition of searching only for horizontal reflectors that the alternative possibility of nearly vertical scatterers should be taken seriously.

5.3. What is the vertical extent of the anomaly?

In view of the potential geodynamical implications, it is important to assess whether the anomaly we detect is indeed vertical, and what its vertical extent is. As mentioned in paper I, it is in principle possible to investigate the depth variation of the anomaly by inverting separately several bands of epicentral distance. Unfortunately, in the case of Hawaii, the coverage is not sufficient to permit this exercise. It could be done in the future as more data get collected at seismic stations in the Pacific, but, at present, we cannot demonstrate any sort of connectivity between the anomaly we find at depth and Hawaii.

Fig. 2 shows that most seismograms we have are sensitive to heterogeneities in the lowest 1000 km of the lower mantle. It is clear that if the anomaly was only present in a small portion of the lower mantle (the D″ layer for example), it would be even more difficult to explain the observed amplitudes [28].

Similarly, if the anomaly was too far from vertical, the scattered signals would loose their coherence. On the other hand, it is very possible that the fact we observe a double slow anomaly is due to a small tilt of the 'plume'. In any case, we cannot resolve these two anomalies independently.

5.4. Further work

Applications of the same technique to the lower mantle beneath Iceland and Bowie are reported elsewhere [28].

A good test of the hypothesis of scattered waves would be to check that these waves arrive at some angle from the great circle. Indeed, our analysis predicts deviations from 30º to 50º. This could be done in two ways: using a local array [20,29], or using the horizontal components of the seismograms. The second possibility is appealing, but it should be noted that these teleseismic scattered waves arrive very steeply beneath the stations (near 15º from the vertical), so that the expected horizontal amplitude is only one fourth of the vertical amplitude.

Further extensions could include the search for P-to-S and S-to-P conversions due to scattering by vertical heterogeneities.

6. Geodynamical implications

Assuming that we are indeed mapping vertical heterogeneities in the lower mantle, we now turn to the geodynamical implications of our results. It is of course tempting to see in the double slow anomaly northwest of Hawaii a mantle plume that feeds the Hawaiian hotspot. This would indicate that the plume model of Morgan [2], with plumes originating in D″, indeed applies to Hawaii. The strength of the anomaly indicates that it cannot be due to temperature effects alone. Partial melt, as inferred from seismological studies of the lowermost mantle [30], could produce the large anomaly we detect. Again, since this would be the first time that a plume is detected in the lower mantle, it is difficult to relate to earlier work. Nevertheless, there has been recent attempts to infer the deep position of plumes, assuming they are entrained in the 'mantle wind'. In Fig. 6, we have plotted on top of our map the predicted plume positions at the CMB for Hawaii, according to two recent studies. While Corrieu-Sipahimalani [13] finds that the Hawaiian plume would originate northwest of Hawaii, Steinberger and O'Connell [14] predict a source far south of Hawaii. Our result favours a source to the northwest, not far from the surface expression of Hawaii. Note that this gives some coherence to our approach, since we assumed in the first place that the plume was nearly vertical to reduce the tomographic problem to two dimensions. However, at present, we cannot demonstrate any sort of connectivity between the anomaly we find at depth and Hawaii.

7. Conclusion

In a companion paper [11] we have developed a new tomographic method to image plume-like structures in the lower mantle. This method is akin to diffraction tomography, and relies on the use of long-period scattered body waves. In this paper, we applied this new technique to the actual available data, in order to image the lower mantle beneath Hawaii. Our maps indicate the presence of a strong slow anomaly deep in the mantle, a few degrees northwest of Hawaii. The anomaly is 30 to 60 times larger than what we predicted in paper I for what we thought was a reasonable thermal plume model. Although we cannot completely rule out that our maps are dominated by artefacts, we performed several tests that suggest that the detected anomaly is real and robust. Because it is the first time that such an approach is taken, it is difficult to be absolutely positive about the existence of the anomaly. If real, it strongly suggests that a mantle plume is responsible for the Hawaiian hotspot, as originally suggested by Morgan [2]. The plume originates in D″, and seems nearly vertical, since its source lies only a few degrees away from its surface expression. However, we cannot prove any sort of connectivity between our deep anomaly and Hawaii, with the presently available data set. The large amplitude of the anomaly indicates that it is not only of thermal origin, and partial melt, or some other enhancing process, must be invoked. We think that diffraction tomography can bring essential informations on the structure of the mantle, and that using

it to detect vertical features represents an original alternative to the traditional search for horizontal reflectors.

Acknowledgements

We thank Michael Weber, Guust Nolet, Thorne Lay, and three anonymous reviewers for useful suggestions, and for expressing their scepticism about our results. Yong Ji benefited of a thesis scholarship from CNRS. Maps have been drawn with the 'P' program developed by Spakman, Govers, de Jonge and Remkes at the University of Utrecht. This research was supported in part by CNRS-INSU 'Tomographie'. ***[RO]***

References

[1] J.T. Wilson, A possible origin of the Hawaiian island, Can. J. Phys. 41 (1963) 863–868.
[2] W.J. Morgan, Convective plumes in the lower mantle, Nature 230 (1971) 42–43.
[3] R.A. Duncan, M.A. Richards, Hotspots, mantle plumes, flood basalts and true polar wander, Rev. Geophys. 29 (1991) 31–50.
[4] H.M. Iyer, J.R. Evans, G. Zandt, R.M. Stewart, J.M. Coakley, J.N. Roloff, A deep low-velocity body under the Yellowstone caldera, Wyoming: delineation using P-wave residuals and tectonic interpretation: summary, Geol. Soc. Am. Bull. 92 (1981) 792–798.
[5] M. Granet, G. Stoll, J. Dorel, U. Achauer, G. Poupinet, K. Fuchs, Massif Central (France): new constraints on the geodynamical evolution from teleseismic tomography, Geophys. J. Int. 121 (1995) 33–48.
[6] J.C. VanDecar, D.E. James, M. Assumpcao, Seismic evidence for a fossil mantle plume beneath South America and implications for plate driving forces, Nature 378 (1995) 25–31.
[7] C.J. Wolfe, I.T. Bjarnason, J.C. VanDecar, C. Solomon, Seismic structure of the Iceland mantle plume, Nature 385 (1997) 245–247.
[8] H.-C. Nataf, J. VanDecar, Seismological detection of a mantle plume?, Nature 364 (1993) 115–120.
[9] E.R. Kanasewich, R.M. Ellis, C.H. Chapman, P.R. Gutowski, Teleseismic array evidence for inhomogeneities in the lower mantle and the origin of the Hawaiian islands, Nature 239 (1972) 99.
[10] C. Wright, Comments on "Seismic array evidence of a core boundary source for the Hawaiian linear volcanic chain" by Kanasewich et al., J. Geophys. Res. 80 (1975) 1915–1919.
[11] Ying Ji, H.-C. Nataf, Detection of mantle plumes in the lower mantle by diffraction tomography: theory, Earth Planet. Sci. Lett. (this issue).
[12] B.L.N. Kennett, E.R. Engdahl, Traveltime for global earthquake location and phase identification, Geophys. J. Int. 105 (1991) 429–465.
[13] V. Corrieu-Sipahimalani, Modèles dynamiques du manteau terrestre: observations et contraintes, Thèse de Doctorat en Sciences, Université de Cergy-Pontoise, 1995.
[14] B. Steinberger, R.J. O'Connell, Advection of plumes in mantle flow; implications for hotspot motion, mantle viscosity plume distribution, Geophys. J. Int. 132 (1998) 412–434.
[15] W. Spakman, Delay-time tomography of the upper mantle below Europe, the Mediterranean, and Asia Minor, Geophys. J. Int. 107 (1991) 309–332.
[16] S.P. Grand, Mantle shear structure beneath the Americas and surrounding oceans, J. Geophys. Res. 99 (1994) 11591–11621.
[17] J.H. Woodhouse, A.M. Dziewonski, Mapping the upper mantle: three-dimensional modeling of earth structure by inversion of seismic waveforms, J. Geophys. Res. 89 (1984) 5953–5986.
[18] R. Van der Hilst, Tomography with P, PP and pP Delay-Time Data and the Three-Dimensional Mantle Structure below the Caribbean Region, Ph.D. Thesis, University of Utrecht, 1990.
[19] P.M. Shearer, Constraints on upper mantle discontinuities from observations of long-period reflected and converted phases, J. Geophys. Res. 96 (1991) 18147–18182.
[20] F. Neele, R. Snieder, Are long-period body wave coda caused by lateral heterogeneity, Geophys. J. Int. 107 (1991) 131–153.
[21] F. Neele, R. Snieder, Topography of the 400 km discontinuity from observations of long-period P400P phases, Geophys. J. Int. 109 (1991) 670–682.
[22] E. Wielandt, On the validity of the ray approximation for interpretating delay times, in: G. Nolet (Ed.), Seismic Tomography, Reidel, Dordrecht, 1987, pp. 85–98.
[23] S. Karato, Importance of anelasticity in the interpretation of seismic tomography, Geophys. Res. Lett. 20 (1993) 1623–1626.
[24] E.J. Garnero, D.V. Helmberger, Seismic detection of a thin laterally varying boundary layer at the base of the mantle beneath the central-Pacific, Geophys. Res. Lett. 23 (1996) 977–980.
[25] R. Gritto, Rayleigh Scattering and Nonlinear Inversion of Elastic Waves, Ph.D. Thesis, University of California at Berkeley, 1995.
[26] M. Korn, Seismic waves in random media, J. Appl. Geophys. 29 (1993) 247–269.
[27] H. Emmerich, J. Zwielich, G. Müller, Migration of synthetic seismograms for crustal structures with random heterogeneities, Geophys. J. Int. 113 (1993) 225–238.
[28] Y. Ji, Tomographie par diffraction et détection de panaches mantelliques dans la manteau inférieur, Thèse de l'Université Paris 7, 1996.
[29] F. Scherbaum, F. Krüger, M. Weber, Double beam imaging:

mapping lower mantle heterogeneities using combinations of source and receiver arrays, J. Geophys. Res. 102 (1997) 507–522.

[30] Q. Williams, E.J. Garnero, Seismic evidence for partial melt at the base of earth's mantle, Science 273 (1996) 1528–1530.